

Article

# A Strain-Based Percolation Model and Triaxial Tests to Investigate the Evolution of Permeability and Critical Dilatancy Behavior of Coal

Dongjie Xue <sup>1,2,3,\*</sup> , Jie Zhou <sup>1</sup>, Yintong Liu <sup>1</sup> and Sishuai Zhang <sup>1</sup>

<sup>1</sup> School of Mechanics and Civil Engineering, China University of Mining and Technology, Beijing 100083, China; cumtb.zhoujie2018@gmail.com (J.Z.); cumtb.liuyintong2018@gmail.com (Y.L.); cumtb.zhangsishuai2018@gmail.com (S.Z.)

<sup>2</sup> State Key Laboratory of Coal Mine Disaster Dynamics and Control, Chongqing University, Chongqing 400030, China

<sup>3</sup> Key Laboratory of Safety and High-efficiency Coal Mining, Anhui University of Science and Technology, Huainan 232001, China

\* Correspondence: xuedongjie@163.com; Tel.: +86-1-15101127335

Received: 5 July 2018; Accepted: 6 August 2018; Published: 13 August 2018



**Abstract:** Modeling the coupled evolution of strain and CH<sub>4</sub> seepage under conventional triaxial compression is the key to understanding enhanced permeability in coal. An abrupt transition of gas-stress coupled behavior at the dilatancy boundary is studied by the strain-based percolation model. Based on orthogonal experiments of triaxial stress with CH<sub>4</sub> seepage, a complete stress-strain relationship and the corresponding evolution of volumetric strain and permeability are obtained. At the dilatant boundary of volumetric strain, modeling of stress-dependent permeability is ineffective when considering the effective deviatoric stress influenced by confining pressure and pore pressure. The computed tomography (CT) analysis shows that coal can be a continuous medium of pore-based structure before the dilatant boundary, but a discontinuous medium of fracture-based structure. The multiscale pore structure geometry dominates the mechanical behavior transition and the sudden change in CH<sub>4</sub> seepage. By the volume-covering method proposed, the linear relationship between the fractal dimension and porosity indicates that the multiscale network can be a fractal percolation structure. A percolation model of connectivity by the axial strain-permeability relationship is proposed to explain the transition behavior of volumetric strain and CH<sub>4</sub> seepage. The volumetric strain on permeability is illustrated by axial strain controlling the trend of transition behavior and radical strain controlling the shift of behavior. A good correlation between the theoretical and experimental results shows that the strain-based percolation model is effective in describing the transition behavior of CH<sub>4</sub> seepage in coal.

**Keywords:** enhanced permeability; deviatoric stress; mechanical behavior transition; CH<sub>4</sub> seepage; volumetric strain; strain-based percolation model

## 1. Introduction

Enhanced coal permeability after failure under triaxial stress can be determined quantitatively by the stress-dependent model. However, the sudden change in permeability from porous to fractured coal is more important in order to understand the enhanced mechanism and improve the stress-relieving technology and hydromechanical (HM) fracturing method. On the other hand, the production of coalbed methane (CBM) as green energy has been increasingly important, particularly in winter 2017, with more determination to fight air pollution in the face of the gas shortage initiative in China [1]. Most of China's coal has high density and low permeability, typically less than 1 mD [2,3]. In coal

seams, to improve permeability for easy extraction, premining the protective coal is often carried out to relieve the stress [4,5]. At the working face, the hydraulic fracturing method is often employed to achieve local stress adjustment. The huge demand in CH<sub>4</sub> promotes a deep understanding of sudden changes in permeability, especially induced by the coupled effect of gas and stress. The key to all these problems is to accurately understand the transition of permeability. We need a new model that can illustrate the whole change in permeability, even sudden transitions.

Under triaxial compression, the permeability of CH<sub>4</sub> mainly depends on the shearing-induced dilatancy of the coal. Modeling enhanced permeability with deviatoric stress is useful for understanding the coupled mechanism between the dilatant deformation and the seepage or percolation channel. Many outstanding achievements focus on the study of stress-dependent permeability without considering transition effect. Many models [6–11], as shown in Table 1, have been made based on the excavation damage zone (EDZ), which depends on continuous media to explain the coupled process [12]. To our knowledge, the stress-dependent model can effectively explain the coupled effect before the dilatant boundary, taking coal as a continuous porous medium, and after, taking coal as discontinuous fractured medium. According to percolation theory, there must be a state transition of the continuous-discontinuous behavior controlling the coal permeability by connected clusters of multiscale networks [10]. The multiscale can be referred as nano, micro, meso, macro, and even mega scale. The corresponding structure of discontinuities changes from pore to fracture. Here, we only focus on the study of cylindrical coal sample in lab. The resolution for pore structure by CT is about 60 μm, which can be the lower limit of size. There will be fracture generation connecting the top and bottom of the coal sample, which is about 12 cm long. The study is based on the multiscale structure from 60 μm to 12 cm, and the upper limit is 2000 times the lower limit. Indeed, the multiscale network of pore-crack-fracture is mainly generated at the dilatant boundary, and the focus of study is on the multiscale behavior and sudden transition of permeability. It is difficult to determine the boundary of two kinds of adjacent pore structures and the scale invariance is often used to understand the multiscale behavior based on the percolation theory. So, the sudden transition in permeability needs a new understanding of phase transition for the continuous-discontinuous behavior.

Considering the transition behavior, the local stress redistribution around isolated fractures changes dramatically, and the deviatoric stress cannot control the sudden increase of volumetric strain and permeability. Eventually, open fractures provide the main path for gas seepage until there is a steady flow. So, the initial permeability  $k_0$  can be determined by Darcy's law [6,7,13] or the Carman-Kozeny equation [14,15]. The final permeability  $k_f$  is often determined by the cubic law [11,13,16] through fissure flow in discontinuous fractured coal. For the transition behavior, there is always a sudden increase of volumetric strain or permeability [17,18]. Meanwhile, the coal changes from continuous to discontinuous, corresponding to the generation of a multi scale network of void structures. In mathematical terms, we can understand such behavior as a continuous and nonderivative relationship. In physical terms, we propose the sudden changes of mechanical behavior from pore-dominated structure to fracture-dominated structure as the phase transition according to percolation theory [19,20]. The initial phase dominated by the continuous behavior moves into the final phase dominated by discontinuous structural behavior. The pore-based material behavior is continuous for Darcy's flow and the fracture-based structural behavior is discontinuous for the cubic law.

Table 1. Stress-dependent models.

Model	Classification	Gas	Lithological Type	Related Theory
$k_f/k_0 = e^{-3 \times 10^{-3} \bar{\sigma} k_0^{-0.1}} + 2 \times 10^{-4} \bar{\sigma}^{1/3} k_0^{1/3}$	Theory and measured data (Somerton et al., 1975)	N <sub>2</sub> CH <sub>4</sub>	Coal	Darcy's law
$k_f = (1.12 - 0.03\sigma_3)K \times e^{-(1.12-0.03\sigma_3)C_f\sigma_3}$	Measured data (Durucan and Edwards, 1986)	N <sub>2</sub>	Coal	Darcy's law
$k_f/k_0 = e^{-3 \times C_f \times \Delta\sigma} / [1 - \phi_0(1 - e^{-C_f \times \Delta\sigma})]$	Theory and measured data (McKee et al., 1988)	CH <sub>4</sub> H <sub>2</sub> O	Coal	Carman-Kozeny equation
$k_f/k_0 = e^{-3 \times C_f \times \Delta\sigma}$	Theoretical solution (Seidle et al., 1992)	H <sub>2</sub> O	Coal	Carman-Kozeny equation
$k_f/k_0 = [(\eta + e^{-C_f\sigma_f}) / (\eta + e^{-C_f\sigma_0})]^3$	Theoretical solution (Liu et al., 2009, 2010)	CH <sub>4</sub>	Coal	Cubic law

Note.  $k_0$  and  $k_f$  mean initial and final permeability corresponding to the initial effect stress  $\sigma_0$  and final effect stress  $\sigma_f$ .  $\Delta\sigma = \sigma_f - \sigma_0$ .  $\bar{\sigma}$  is the mean stress and  $\sigma_3$  is the confining pressure.  $K$  defines the relative coefficient of existing fractures,  $C_f$  represents the compressibility of coal, and  $\eta$  defines the influence of the effective stress induced closure of aperture.

Therefore, it is necessary to establish a new model that will help us understand transition behavior in permeability. Percolation theory [21–24] is very effective at explaining such phase transitions in disordered media. For coal under conventional triaxial compression, the continuous-discontinuous transition depends on the cluster generation of multiscale pore-crack-fracture, as well as the structural phase transition behavior of the connected clusters. Percolation models have been used to analyze the fracture-induced transitions of various rocks [23–26]. However, due to our limited knowledge, there has been almost no analysis of CH<sub>4</sub> flow considering the mechanical-structural transition in coal.

Another focus is the multiscale geometric topology of the network that influences percolation depending on the generation, distribution, and opening of fractures. It is impossible to find the exact solution of local stress near all fractures, which dominate local opening and closing. The topology evolution can be considered by the equivalent strain of coal considering the discontinuities. We mainly focus on the percolation model of strain-dependent permeability by designing a series of orthogonal experiments of conventional triaxial compression for coupled stress-strain permeability.

## 2. Materials and Experimental Methods

### 2.1. Coal Sample Preparation for Orthogonal Experiments

The coal blocks in China were selected at a depth of 690 m, and the coal seam has an average thickness of 3.5 m with an inclination of 23°. The roof and floor of the roadway are fine-grained sandstone. Then, the coal blocks were processed into cylinder-shaped samples with a standard size of 50 mm diameter × 100 mm height [27]. The 9 samples were numbered C01, C02, C03, C04, C05, C06, C07, C08, and C09.

Figure 1 illustrates the designed cycle of experimental procedures for coupled research including the determined physical parameters, the multiscale structures by computed tomography (CT) before and after failure, and triaxial compression coupled with CH<sub>4</sub> seepage. Triaxial servo-controlled seepage equipment for coupled thermo-fluid-solid of coal was adopted for the coupled behavior. The system collected data at 1 s intervals, automatically recording axial force, axial and radial displacement, confining pressure, temperature, and gas flow. After the samples were dried in an oven for 12 h, their height, area, and porosity were measured, as shown in Table 2.



Figure 1. Experimental design.

**Table 2.** Physical parameter determination. Porosity is measured by computed tomography (CT) after failure.

Samples	Height	Cross-Section Area	Volume	Dry Weight	Density	Porosity
	/cm	/cm <sup>2</sup>	/cm <sup>3</sup>	/g	g/cm <sup>3</sup>	%
C01	10.40	19.63	204.15	279.0	1.37	4.83
C02	10.56	19.63	207.29	281.5	1.36	3.32
C03	10.50	19.63	206.12	276.7	1.34	3.13
C04	10.50	19.63	206.12	269.8	1.31	1.44
C05	10.27	19.63	201.60	299.0	1.48	4.87
C06	10.56	19.63	207.29	279.3	1.35	1.17
C07	9.44	19.63	185.31	250.2	1.35	6.02
C08	10.40	19.63	204.15	269.2	1.32	8.25
C09	10.52	19.63	206.51	278.9	1.35	4.32

Then, the coupled tests were carried out. To prevent gas leakage through the sidewalls, they were covered with a 1 mm thick layer of silica gel. Sliding the heat-shrink tubing over the surface keeps the gel in close contact with the sidewalls, preventing the hydraulic oil from penetrating into the samples. After that, the extensometer for radial displacement was installed and the flow meter was connected. The outlet valve was closed after removing the air from the chamber with a vacuum pump, filling it with CH<sub>4</sub> and allowing 24 h for adsorption equilibrium. We then started the system and imposed displacement controlled axial stress load at a rate of 0.1 mm/min. Table 3 shows the designed orthogonal experiments with confining pressures of 3 MPa, 6 MPa, and 9 MPa, and gas pressures of 1 MPa, 1.5 MPa, and 2 MPa.

**Table 3.** Experimental design by orthogonal stress.

Sample	Confining Pressure	Inlet Gas Pressure	Dilatant Stress and Strain		Peak Stress and Strain		Residual Stress and Strain		Permeability		Stress Ratio
	$\sigma_3$	$p_1$	$\sigma_D$	$\varepsilon_D$	$\sigma_P$	$\varepsilon_P$	$\sigma_R$	$\varepsilon_R$	$k_0$	$k_f$	$\sigma_D/\sigma_P$
C01	9	1	22.77	0.45	43.12	−0.31	21.58	−6.45	3.93	56.96	0.53
C02	6	1.5	17.30	0.38	35.62	−1.05	26.77	−9.01	16.75	31.73	0.49
C03	3	2	18.08	0.39	25.83	0.17	19.04	−4.56	0	2434	0.70
C04	9	1.5	25.25	0.67	39.39	−1.14	31.59	−4.78	65.75	27.17	0.64
C05	6	2	22.01	0.44	43.12	−4.03	21.58	−6.44	11.07	1086	0.51
C06	3	1	24.37	0.63	39.20	−0.14	29.53	−4.50	187.5	51.87	0.62
C07	9	2	27.38	0.45	50.78	0.19	33.43	−2.51	0	Failed	0.54
C08	6	1	27.36	0.51	40.53	−0.59	26.15	−8.25	375.2	3653	0.68
C09	3	1.5	35.90	0.80	42.06	0.25	39.60	−4.20	0	4343	0.85

Note.  $\sigma_3$ ,  $p_1$ ,  $\sigma_D$ ,  $\sigma_P$  and  $\sigma_R$  have the same unit of MPa.  $\varepsilon_D$ ,  $\varepsilon_P$  and  $\varepsilon_R$  have the same unit of %.  $k_0$  and  $k_f$  have the same unit of  $10^{-18}$  m<sup>2</sup>.

## 2.2. CT Observation of Multiscale Structures

Before the coupled test for permeability, the samples were scanned using an industrial CT scanner. A random zone of 30 mm to 35 mm from the bottom was determined as the interesting area, and the scan interval was set at 0.1 mm, with a total of 51 layers, shown in Figure 2. After sample failure, the same zone of all 9 samples was scanned again for CT images of 1024 × 1024 pixels and 57 μm resolution.



Figure 2. CT scan of interesting area.

### 2.3. Theory of $\text{CH}_4$ Seepage in Coal

Coal is often described as a dual-porosity medium considering the multiscale effect. When there is  $\text{CH}_4$  flow in the multiscale network, an assumption of isothermal seepage in coal is often given as the ideal gas. The gas flow rate is automatically recorded and the permeability at different points can be determined by Darcy's law [28,29]:

$$k = \frac{2qp_0\mu L}{A(p_1^2 - p_2^2)} \quad (1)$$

where  $q$  is the flow rate (m/s),  $k$  is the permeability ( $\text{m}^2$ ),  $p_0$  is the atmospheric pressure (0.1 MPa),  $A$  is the cross-sectional area ( $\text{m}^2$ ),  $\mu$  is the gas viscosity coefficient ( $1.087 \times 10^{-5} \text{ Pa} \cdot \text{s}$ ) at  $20^\circ\text{C}$ ,  $L$  is the height of the cylinder (m), and  $p_1$  and  $p_2$  are gas pressure at the air inlet and outlet, respectively (MPa).

## 3. Experimental Results and Analysis

### 3.1. Effect of Volumetric Deformation on $\text{CH}_4$ Seepage

Figure 3 shows the coupled evolution of permeability with volumetric strain. The nine samples experienced the same behavior, including linear elastic compression, nonlinear compression with local damage, plastic deformation, and post-peak softening before failure. Accordingly, the volumetric strain underwent the two main stages, compression and dilatancy. There are two kinds of transition point: the first is the dilatant point, indicating the deformation transition from compression to dilatancy, and the second is the continuous-discontinuous point, indicating the phase from pore-based to fracture-based structure. The confining pressure promotes strain-softening behavior in the post-peak deformation. The higher the confining pressure, the more likely that volumetric strain will increase nonlinearly with stress.

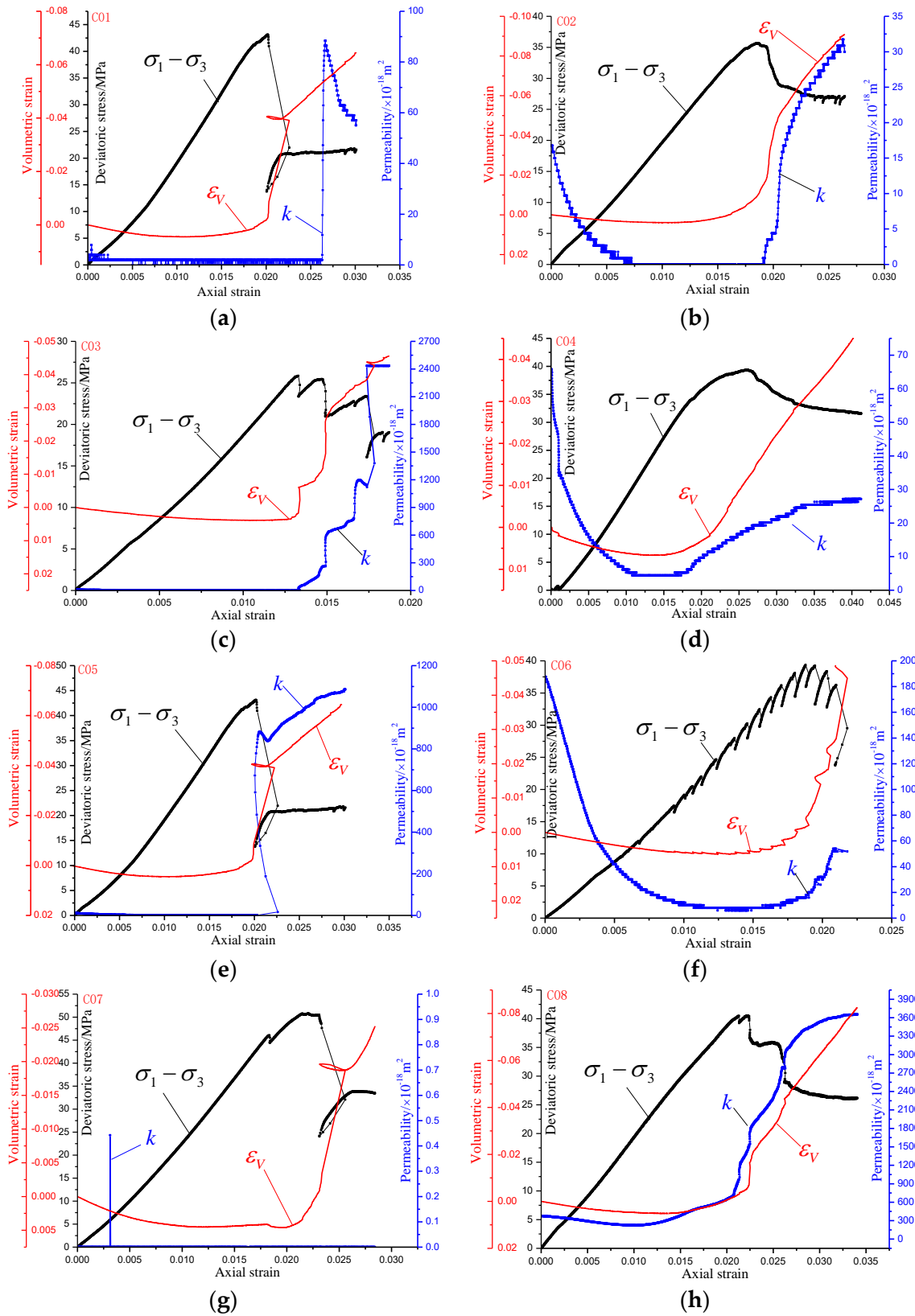
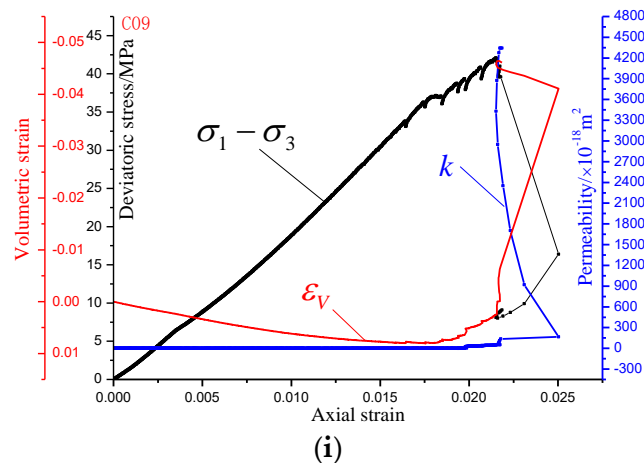


Figure 3. Cont.



**Figure 3.** Evolution of volumetric strain and permeability on samples (a) C01, (b) C02, (c) C03, (d) C04, (e) C05, (f) C06, (g) C07, (h) C08, and (i) C09. Black lines indicate the stress–strain relationship, red lines indicate the volumetric–axial strain relationship, and blue lines indicate permeability with axial strain.

The permeability evolution with deviatoric stress can be determined according to Equation (1), and it shows high consistency with volumetric strain. The initial permeability  $k_0$  for different samples varies, as shown in Table 2. For C01, C03, C05, C07, and C09,  $k_0$  is close to 0. For C02 and C04, it is measured at  $10^{-17} \text{ m}^2$ , and for C06 and C08, it is at  $10^{-16} \text{ m}^2$ , which can be considered low-permeability coal. Increasing deviatoric stress often causes pores to open and fractures to form. Since the volumetric change of a solid matrix is much smaller than the discontinuous geometric structures (e.g., pores, cracks, and fractures), the volumetric strain can be a multiscale variable to illustrate the discontinuous geometries.

When the deviatoric stress is low, low-permeability coal can be considered as a porous medium with preexisting pores under compression. The corresponding volumetric strain decreases, seepage channels close, and permeability decreases. When it reaches the dilatant point, an increase in deviatoric stress will cause crack generation, maintaining volumetric compression, and the channels of the multiscale network are not completely connected. Until the linear–nonlinear transition in volumetric strain, permeability starts to increase significantly. Nonlinear deviatoric stress can be considered as a mechanical phase in percolation theory, in which geometric channels tend to interconnect. During the post-peak stage, fractures connect through the coal sample with a typical stress drop corresponding to strain softening. Fracture geometries, which determine the change of volumetric strain, show a sharp and dramatic increase in dilatancy and seepage. At the end, with the stabilization of residual stress, permeability remains constant. Meanwhile, the confining pressure still has a constraint effect on fracture channels. Therefore, the ultimate permeability is not necessarily greater than the initial value for all samples, such as C04 and C06. There is another possible reason that shear-induced fractures often have an off-axial fracture angle and the connected fracture cannot effectively connect the upper and lower ends of the surface.

### 3.2. Effect of Confining Pressure on Deformation and $\text{CH}_4$ Seepage

During the complete stress–strain evolution, dilatant stress represents nonlinear dilatancy, peak stress indicates coal strength, and residual stress indicates strain-softening behavior. Corresponding to volumetric deformation, there are dilatant strain, peak strain, and residual strain, respectively. Furthermore, permeability changes consistently with nonlinear deformation, and the corresponding points are dilatant permeability, peak permeability, and residual permeability.

The change rates of stress, deformation, and permeability are influenced by the coupled effect of confining pressure and gas pressure. Thus, the stress drop rate can be illustrated by the percentage of stress drop relative to the peak value, the volumetric strain change rate by the percentage of

initial to final volumetric strain, and the permeability change rate by the percentage of initial to final permeability.

With increasing confining pressure, peak stress increases accordingly, as shown in Figure 4a,c. However, both the randomness in sampling and the inhomogeneity influence the peak stress; for example, the peak stress of sample C02 was the lowest when gas pressure was 1.5 MPa, shown in Figure 4b. There is no significant correlation between dilatant stress or residual stress and confining pressure. According to the Griffith crack theory, dilatant stress is mainly influenced by nonlinear deformation and damage accumulation. After the peak strength, the stress drop with discontinuous fractures dominates the residual stress. The increasing confining pressure has an inhibiting effect on dilatancy, while the heterogeneity of fractures determines that the effect under a confining pressure of 9 MPa is not significant.

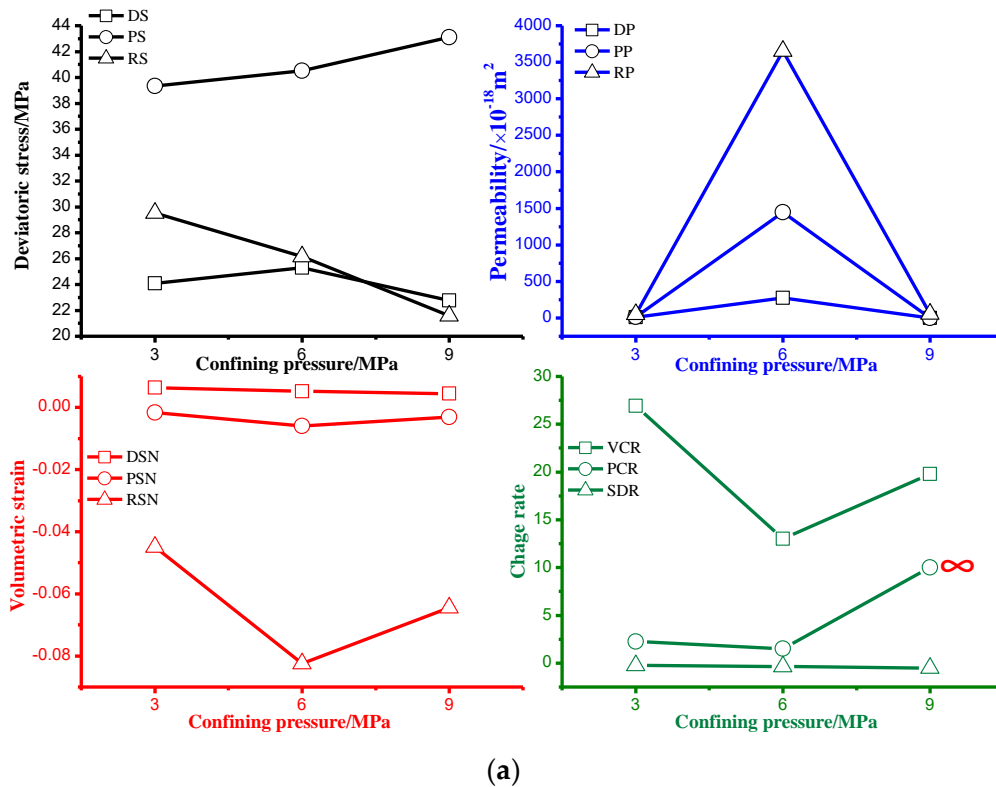
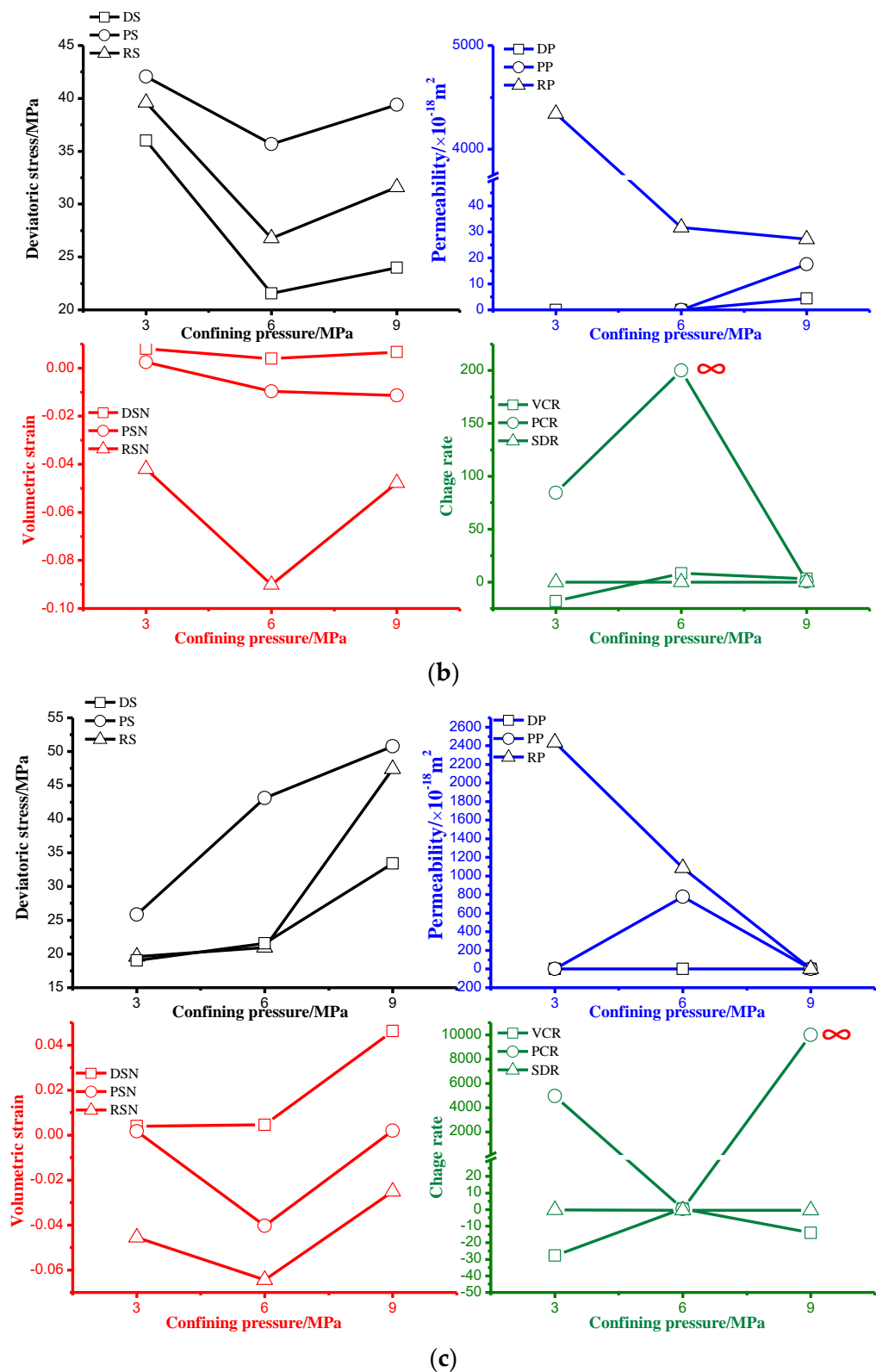


Figure 4. Cont.



**Figure 4.** Deviatoric stress, volumetric strain, permeability, and permeability change rate at dilatant point, peak point, and residual point under confining pressures of (a) 1 MPa, (b) 1.5 MPa, and (c) 2 MPa. ∞ indicates an infinite value because the denominator may be 0, represented by a larger value such as 200 or 10,000.

Positive dilatant strain means a state of compression, and confining pressure does not increase significantly. Peak strain changes slightly with an increase in confining pressure. Residual strain largely changes in the same trend as peak strain. Residual strain is much greater than peak strain, and post-peak volumetric strain increases rapidly, as shown in Figure 4.

Change in volumetric deformation is mainly due to the interconnection of the multiscale network, and the nonlinear volumetric deformation leads to a change in permeability, not the linear change. In spite of the heterogeneity of the different samples, overall, confining pressure has a significant inhibiting effect on permeability, with residual permeability being the highest, peak permeability next, and dilatant permeability the lowest, even as low as 0. During the post-peak stage, volumetric strain and permeability change significantly. The change rates of volumetric strain and permeability are highly consistent, but have low correlation with confining pressure.

### 3.3. Effect of Gas Pressure on Deformation and $CH_4$ Seepage

According to the principle of effective stress, the enclosed gas pressure can reduce the net value of external pressure on the coal matrix. Overall, with an increase in gas pressure, dilatant stress, peak stress, and residual stress all increase accordingly. With an increase in confining pressure, the enclosed space tends to be ideal and the three types of stress show a much more significant increase, as shown in Figure 5. In most cases, residual stress is greater than dilatant stress. After peak stress, the enclosed space is broken and the static pressure in the porous network does not play a determining role, while under dilatant stress, the sample is still in a nonlinear enclosed space and pore pressure does not effectively cause an increase. Such difference indicates that pore pressure plays a less significant role than confining pressure. For the applicable conditions of the principle of effective stress, there is an available-to-unusable transition corresponding to the enclosed space existing and breaking after failure.

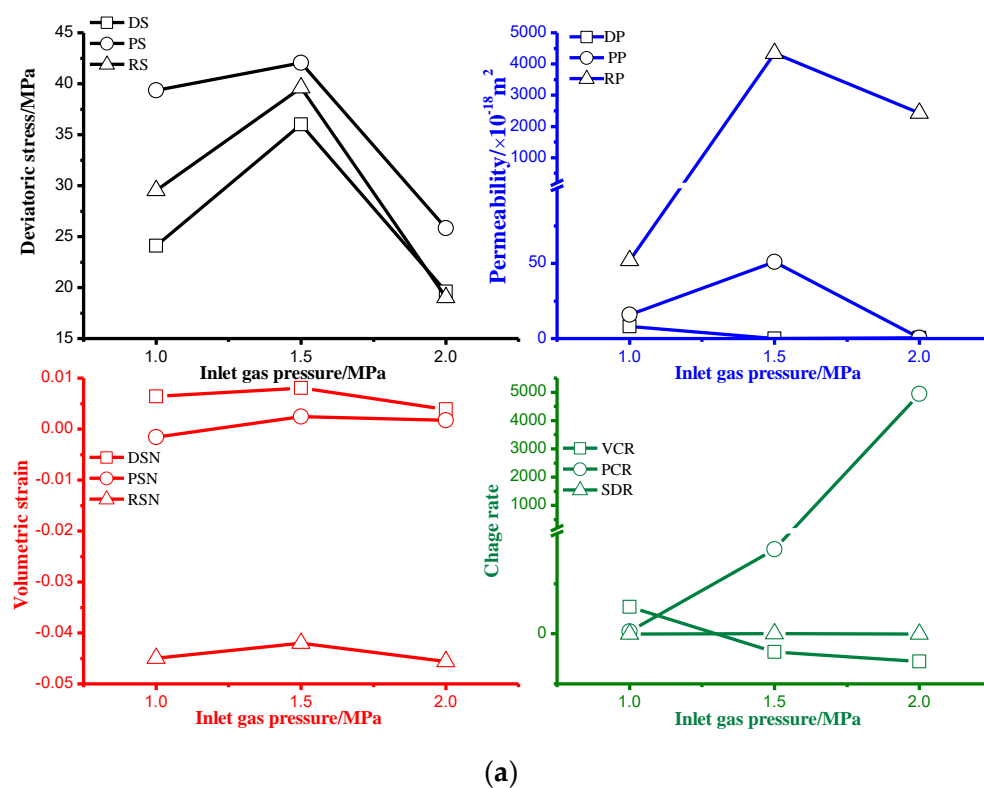
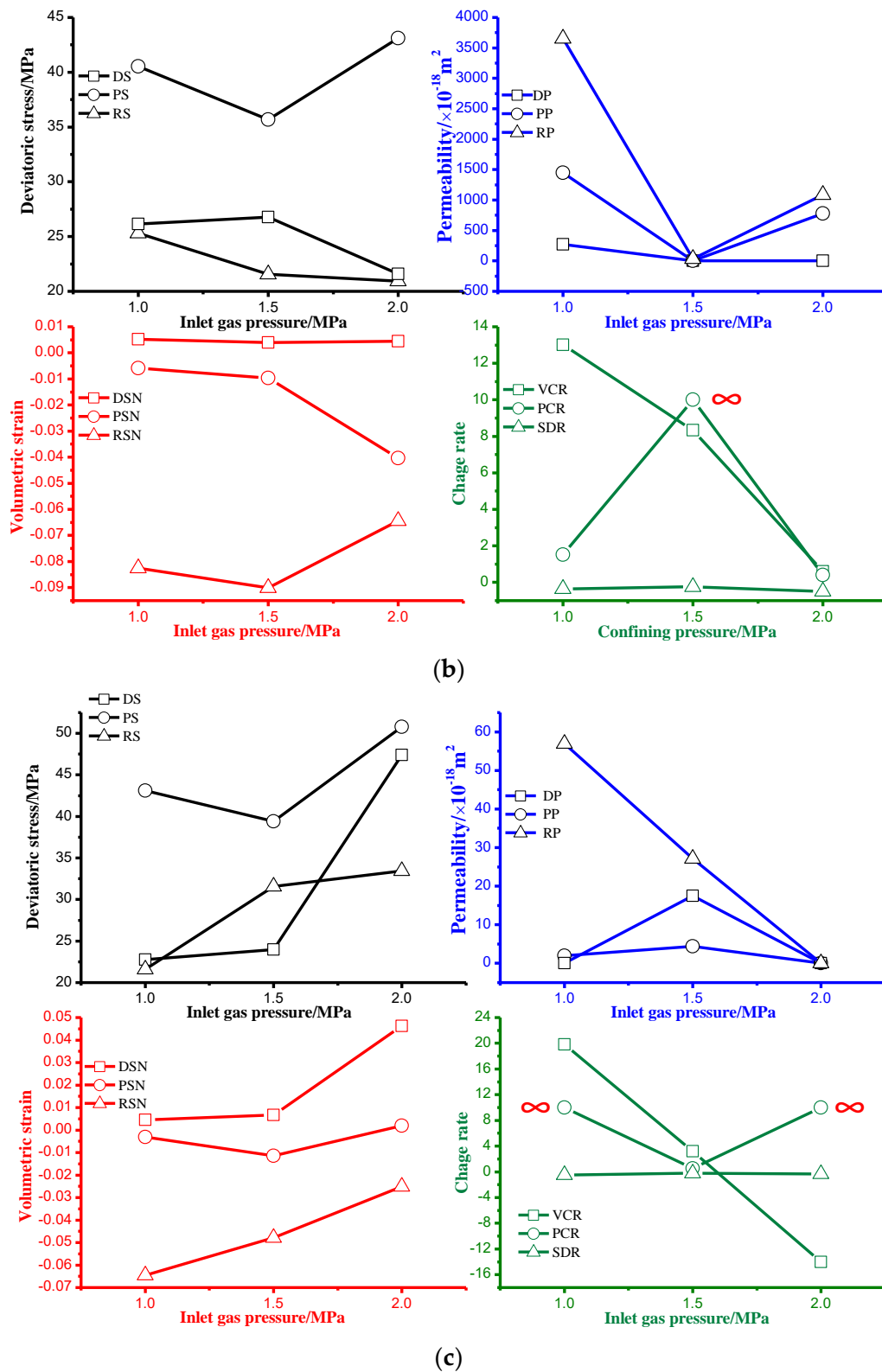


Figure 5. Cont.



**Figure 5.** Deviatoric stress, volumetric strain, permeability, and permeability change rate at dilatant point, peak point, and residual point under confining pressures of (a) 3 MPa, (b) 6 MPa, and (c) 9 MPa ∞ indicates an infinite value because the denominator may be 0, represented by a larger value such as 10.

Volumetric change under different pore pressures is not significant, and dilatant strain experiences no change. Therefore, the change in peak strain and residual strain is mainly due to deviatoric stress. Permeability changes in a similar way to volumetric change. The sensitivity of pore pressure on the rate of volumetric strain and permeability is greater than the stress drop.

Coal deformation includes continuous deformation of matrix influenced by effective stress, pore deformation influenced by pore pressure, and discontinuous deformation of fracture influenced by deviatoric stress. Based on triaxial compression, before the dilatant strain, coal can be considered as a porous medium, dominated by matrix deformation and pore deformation, and the principle of effective stress is met in the enclosed pore space. After dilatant strain, nonlinear deformation promotes the development of a multiscale network, including pore interconnection and fracture generation. After peak strain, the deformation is mainly due to discontinuous fracture connection, and the principle of effective stress is no longer applicable in the broken enclosed space. Before peak strain, deviatoric stress and effective stress dominate the deformation continuously. After, deviatoric stress dominates the structural deformation by discontinuous fractures. Confining pressure and pore pressure can be external stress factors, and the complicated distribution and formation of discontinuities of the multiscale network are internal factors. External stress controls coal deformation by the local stress influenced by internal factors.

#### 4. Percolation Model for Critical Behavior of CH<sub>4</sub> Seepage

##### 4.1. CT Reconstruction of Network and Determination of Fractal Dimension

The CT topography of fractures for all nine samples is shown in Figure 6. After failure, the discontinuities can be divided into micropore network and macro-shear fractures. The complicated distribution of discontinuities shows the strong multiscale effect, and the multiscale connection forms a shearing block. Under triaxial compression, shear stress dominates the connected fracture generation and the shear in 3D space can occur in multiple fracture planes resulting in single network (C01 and C04), multiple network (C02 and C03), bending network (C06), crossed network (C07 and C08), pore-dominated network (C05), and complex network (C09).

Fractal dimension is often used to measure the roughness of a fracture surface, and spatial roughness reflects the complexity of the distribution of shear planes. In this study, we propose a self-similar fractal method [30], i.e., the volume-covering method, to characterize the roughness of a fracture surface. The fundamental concept here is to replace specific grid-covered shape with volume.

For a fractal set  $F$ , most researchers would use the  $n$ -dimensional ball or another collection method such as measuring fractal box scales. A collection of box dimension, often with an easy-to-use and less restrictive concept of  $s$ -dimensional tolerance degree, has a close relationship to volume. To illustrate this point,  $F_\delta$  of  $\delta$  parallel to the body is defined by:

$$A_\delta = \{x \in R^n : |x - y| \leq \delta, \forall y \in A\} \quad (2)$$

So, the definition of  $F_\delta$  of  $\delta$  parallel to the body includes all points set at less than distance  $\delta$ . For example, in the space  $R^3$ , assuming a single point of collection  $F = \{x_0\}$ , there is a sphere of radius  $\delta$  and center coordinates  $x_0$ ; assuming a line segment of collection  $F = \{x_0\}$ , there is a cylinder with the center line  $F$ . The  $n$ -dimensional volume of  $F_\delta$  can be expressed by  $vol^n(F_\delta)$  considering the speed of convergence under the condition  $\delta \rightarrow 0$  with

$$vol^n(F_\delta) \sim c\delta^{n-s} (\delta \rightarrow 0) \quad (3)$$

where  $s$  denotes the dimension of  $F$  and  $c$  can be taken as the  $s$ -dimensional tolerance in set  $F$ .

The three-dimensional volume of  $F_\delta$  could be expressed by  $vol^3(F_\delta)$  considering the speed of convergence under the condition  $\delta \rightarrow 0$  with form

$$\frac{vol^3(F_\delta)}{\delta^3} \sim c\delta^{-s}, (\delta \rightarrow 0) \quad (4)$$

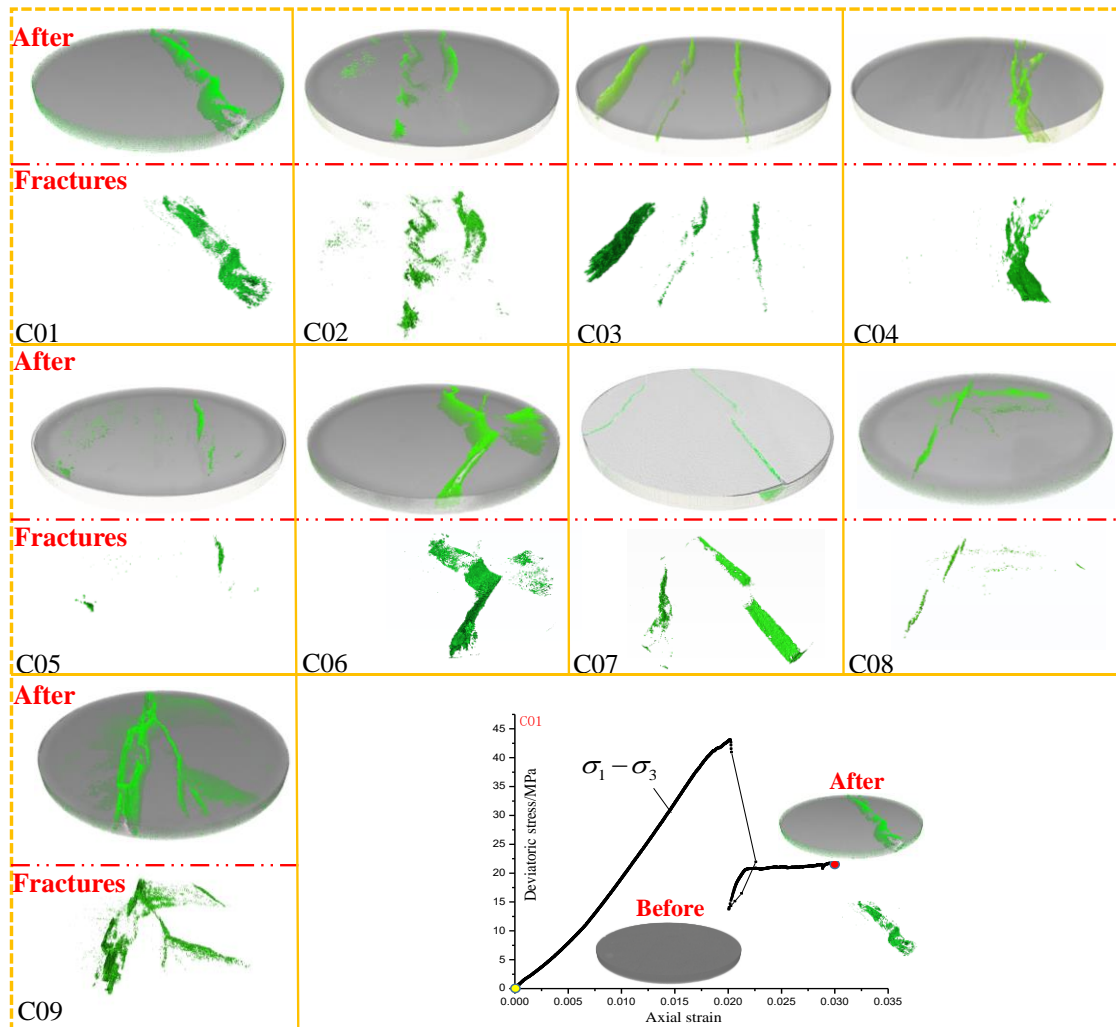


**Figure 6.** CT topography of multiscale network. Yellow and red points indicate CT before and after failure, respectively. C01 and C04 are single network, C02 and C03 are multiple network, C06 is bending network, C07 and C08 are crossed network, C05 is pore-dominated network, and C09 is complex network.

To extend the meaning of the cubic volume  $\delta^3$ , there is the definition of  $v(\delta)$  with the condition  $\lim_{\delta \rightarrow 0} v(\delta) = 0$ . On the whole, the prism-like volume, including the rough surface, could be covered by the volume of  $v(\delta)$  instead of the cubic shape to calculate all the numbers. The total number  $N_{i,j}$  of volume covering one prism-like volume within grid  $(i, j)$  could be expressed by

$$N_{i,j} = INT\left(\frac{vol^3(F_\delta)}{v(\delta)} + 1\right) \quad (5)$$

So, the total number  $N$  of volume covering all prism-like volume could be calculated by

$$N(\delta) = \sum_{i,j=1}^{n-1} N_{i,j} \quad (6)$$

By changing the scale of observation, the total number  $N$  could be calculated repeatedly. Based on fractal theory, the rough surface has fractal properties that strictly follow the relationship

$$N(\delta) \sim c\delta^{-s} \quad (7)$$

According to the volume-covering method, the relationship between fractal dimension  $D$  and porosity  $\phi$  (Table 2) of rough fractures after failure is obtained, shown in Figure 7. The relationship shows good linear characterization with fractal dimension and porosity, verifying that the fractal dimensions can be used to quantitatively characterize the complexity of the spatial distribution of rough fractures.

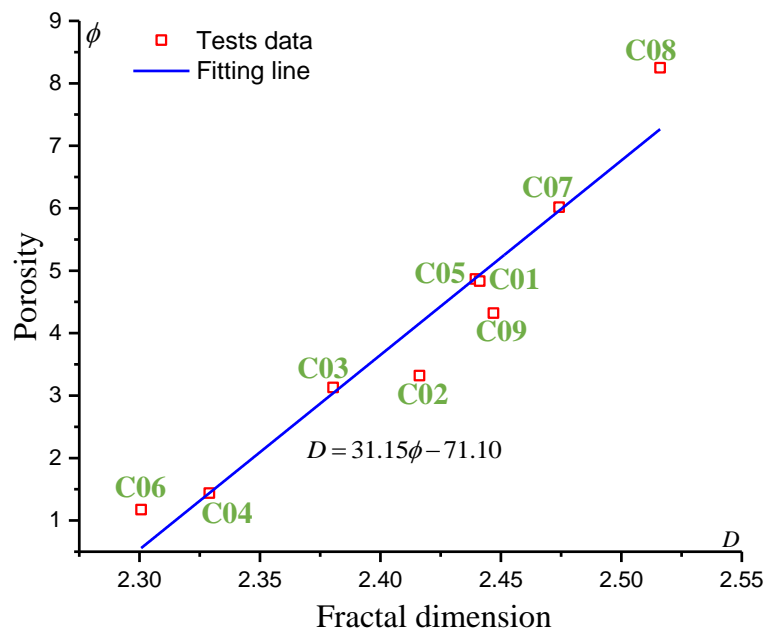


Figure 7. Relationship between fractal dimension and porosity of rough fractures.

#### 4.2. Probability of Multiscale Connectivity Defined by Strain-Based Damage

Under triaxial compression, spherical stress and deviatoric stress both increase. Before the dilatancy boundary, compression is mainly induced by spherical stress with the multiscale network closed. After, deviatoric stress starts to play a role in the open network. In addition, the multiscale behavior influenced by the network connection promotes increasing dilatancy. The deviatoric stress-induced dilatancy and contact surface of asperity decreasing is the main reason for enhanced permeability. Such explanation cannot quantitatively reveal the rapid increase until the network is connected. Indeed, the new interconnection channels by the deviatoric stress-induced deterioration of coal, which connect isolated pores into clusters, are the basis for the sudden transition behavior in permeability.

Moreover, volumetric strain can be used to describe the interconnectivity of the multiscale network indirectly, as shown in Figure 3. There is an increase in damage with shear stress, as well as

the growing multiscale network in coal. Based on axial strain, damage  $D$  induced by deviatoric stress can be defined as:

$$D = \frac{\varepsilon_1}{\varepsilon_{1D}} \quad (8)$$

where  $\varepsilon_1$  is the axial strain corresponding to axial stress  $\sigma_1$  and  $\varepsilon_{1D}$  is the critical axial strain at the dilatant boundary.

When the damage reaches the value of 1, the stress–strain relationship turns from increasing into decreasing, indicating that strengthen behavior changes into strain-softening. The volumetric strain with axial strain also shows the sudden increase at the boundary as well as permeability. We can understand that the transition behavior is caused by the sudden connection of multiscale networks corresponding to the volumetric behavior shifting from compression to dilatancy. With the complete connection of multiscale networks in coal, the probability of  $\text{CH}_4$  flow through the coal increases. Without micropores in the linear deformation, we mainly focus on the permeability evolution influenced by nonlinear deformation.

Clusters are formed by connecting adjacent pores, with an increase in local damage. Then, the clusters keep connecting to each other to form a bigger multiscale network. The connectivity of two pores can be defined as the number of paths allowing  $\text{CH}_4$  to flow as well as the two clusters, even two networks. On a different scale, the number is different and its evolution with the damage is scale invariance [21–24]. Based on the percolation model, we can understand the phenomenon of phase transition caused by the multiscale network [20,26].

When the percolation threshold of network connectivity is reached, permeability increases drastically. The transition of connectivity means the phase of coal changes from porous to fractured medium. By taking the void generation and connection between them as sites and bonds in the percolation modeling, the probability of connectivity  $P$  can be defined as:

$$P \propto (p - p_c)^\beta \quad (9)$$

where  $p$  and  $p_c$  mean the cause of phase transition of connectivity, which is defined as the probability of the occupied lattice of a detailed parameter, i.e., void density  $\rho$  or volumetric strain, and critical probability, respectively.  $\beta$  is a conductivity index of 2 considering the 3D effect [31–33].

Void density is defined as the number of sites in a covering element, and it is also influenced by the multiscale network. As for the sharply increasing transition, crack density instantaneously changes with axial stress, confining pressure, and gas pressure. Its evolution depends on the spatial topology of the network's distribution, generation, and connection. Determination of density can be obtained quantitatively by CT technology. CT is often used to describe the micropore structure in coal, and the phase transition of multiscale structure may adapt the same way.

The final CT topography of the multiscale network can be easily obtained, as shown in Figure 6. The multiscale effect indicates that the scale-dependent variables should be taken into consideration. The critical behavior often shows self-similarity and scale invariance, and fractal theory is often used to describe the similarity of the disordered structures. The linear relationship of the fractal dimension by the volume-covering method and porosity, shown in Figure 7, indicates the self-similarity of the network. The fractal dimension has the same scale invariance as the conductivity index  $\beta$  in percolation theory. Therefore, we can define the multiscale structure of this nature as fractal percolation.

#### 4.3. Percolation Model for Transition Behavior of $\text{CH}_4$ Seepage

Multiscale and quantitative descriptions of conductivity are normally based on permeability and correlate with connected clusters. The geometric opening and closing of pore-crack-fracture are determined by the competition behavior between normal stress-induced compression and shear stress-induced dilatancy. Indeed, shear stress can cause slipping behavior with opening of the contact at the aperture scale, and the improved permeability enhances conductivity.

The evolution of stress-strain-connectivity-conductivity-permeability is stress-dependent permeability, or stress-permeability for short [34]. Many results of stress-permeability show a good fitting relation before failure without strain-connectivity-conductivity. When coal as a porous medium changes into a fracture-dominated structure, few results of stress-permeability can illustrate the sudden transition of the geometric phase. Darcy's law can describe the seepage behavior in porous media, and the cubic law is the theoretical basis for analyzing stress-permeability for fractures [35–37]. For steady flow, the two laws can well describe before and after the dilatant boundary. Based on the steady state of stress, stress-permeability can have good applicability. When at the dilatant boundary, brittle failure with decreasing stress and unchanged strain indicates that stress-permeability is invalid to describe the abrupt change in permeability. Indeed, using stress-induced strain for the direct variable as a geometric factor for permeability and strain-permeability needs more consideration.

It is difficult, if not impossible, to precisely measure and quantify the aperture of multiscale networks. Alternatively, strain can be measured directly and has an advantage of taking into consideration all complicated factors. Establishing strain-permeability may be a more effective method. The relationship between the probability of connectivity and permeability can be defined as:

$$P \propto \frac{k}{k_f} \quad (10)$$

The percolation model for a multiscale network depends on volumetric strain and can be established by triaxial compression of coal. Volumetric strain at the dilatant boundary, shown in Table 3, is determined by axial strain and radial strain. Therefore, critical probability  $p_c$  can be expressed as:

$$p_c \propto \varepsilon_{1D} + \zeta(\varepsilon_{3D}) \quad (11)$$

where  $\varepsilon_{1D}$  is critical axial strain at the dilatant boundary and determines the trend of the percolation curve and  $\zeta(\varepsilon_{3D})$  represents the effect of radial strain and determines the shift of the trend.

The probability density function of axial strain can be used for the multiscale analysis of percolation structures. Therefore, the corresponding occupied probability is:

$$p = 1 - \exp\left(-\frac{\varepsilon_1}{\varepsilon_{1D}}\right) \quad (12)$$

When the multiscale structure reaches the critical state corresponding to  $\varepsilon_{1D}$ , then the critical percolation can be defined as:

$$p_c = 1 - e^{-1} = 0.63 \quad (13)$$

With Equations (9), (10), (12), and (13), the permeability relationship under percolation theory can be obtained as:

$$k = Ck_f \left[1 - e^{-(\varepsilon_1/\varepsilon_{1D})} - 0.63\right]^2 \quad (14)$$

where  $C$  is a constant with a value of 40, which is obtained from the fitting curve in Figure 8.

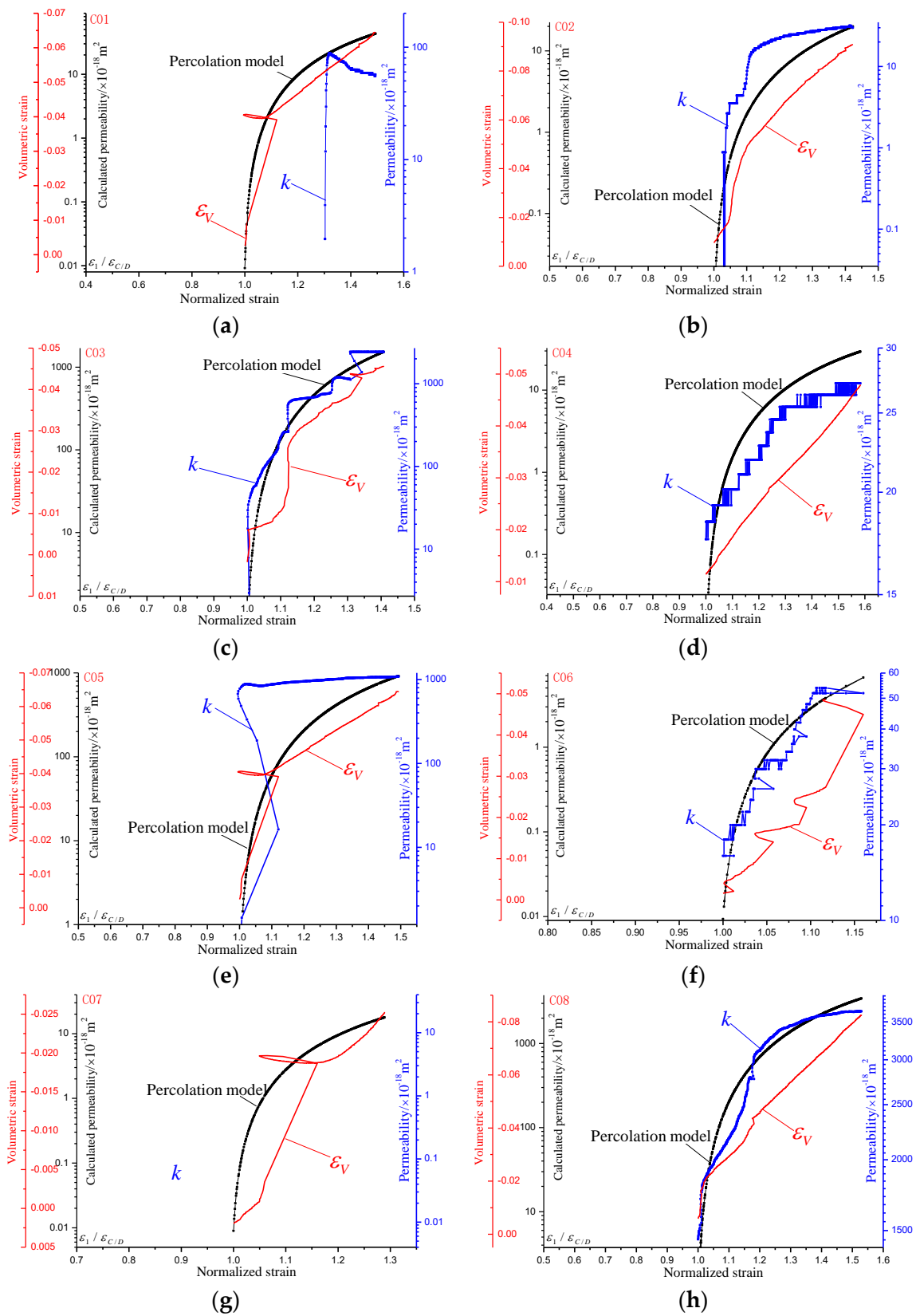
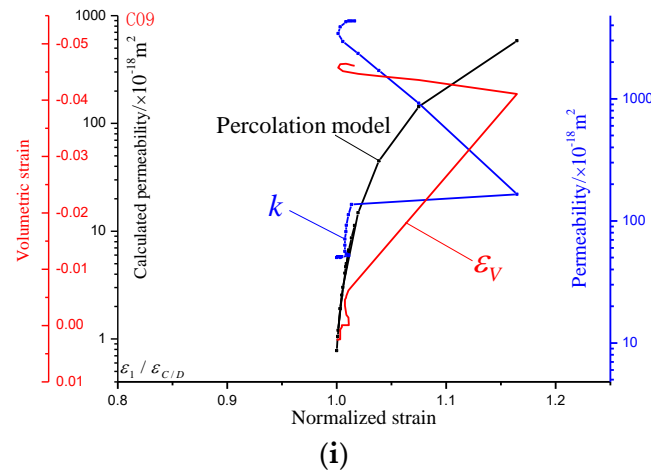


Figure 8. Cont.



**Figure 8.** Percolation model validation and comparison with the experimental data for samples (a) C01, (b) C02, (c) C03, (d) C04, (e) C05, (f) C06, (g) C07, (h) C08, and (i) C09. Black lines indicate the percolation model, red lines indicate the volumetric-normalized strain relationship, and blue lines indicate permeability with normalized strain.

Using Equation (14), we compare the theoretical model with the experimental data for the permeability of all nine samples under triaxial compression. In Figure 8, the effective permeability of C07 is not obtained experimentally. The results for the remaining samples show acceptable matches, and even satisfying matches for C02, C03, C04, C06, and C08. Although confining pressure and gas pressure boundaries are different for each sample in Figures 4 and 5, the percolation model for CH<sub>4</sub> in coal shows excellent effectiveness.

## 5. Conclusions

In this study, the multiscale network is reconstructed by CT technology and determined quantitatively by fractal theory according to the volume-covering method proposed. The coupled tests are carried out by orthogonal experiments of confining pressure and gas pressure. The evolution of CH<sub>4</sub> seepage is modeled by percolation theory for the coupled strain-permeability. The main conclusions are drawn as follows:

1. The gas-stress coupled experiment was carried out for ineffectiveness of the stress-dependent model of permeability at the dilatant boundary. The results show that before failure, coal, as a porous medium, can be coupled with CH<sub>4</sub> seepage by the Darcy's flow, and after failure, coal as a fractured medium can be solved by the cubic law. The closed space before and after failure is the key controlling the assumptions for the law. The stress-dependent model is only effective based on the representative volume element as the continuous medium. The results also show that breakage of the closed space at the dilatant boundary will cause the multiscale behavior, with a sudden increase in volumetric strain and permeability.
2. The coupled strain-permeability of orthogonal experiments on confining pressure and gas pressure was investigated. The results show that there is not good agreement between deviatoric stress, volumetric strain, permeability, change rate, and confining pressure and pore pressure. Almost all the samples have a highly consistent relationship between volumetric strain and permeability at the dilatant point, peak point, and residual point of the stress-strain curve.
3. CT-based reconstruction of multiscale networks in coal at the dilatant boundary is proposed. The results of all samples show various kinds of multiscale networks, and the isolated micropores can be neglected in the linear deformation for the transition of permeability. The shear stress induced by nonlinear deformation of the network should receive more attention.

4. The fractal percolation model of the multiscale network by shear stress is verified by the volume-covering method. The linear relationship between porosity and fractal dimension by the volume-covering method shows the multiscale effect and effective description by fractal theory. The scale invariance of void density, connectivity, and conductivity suggests the percolation model's understanding of the coupled behavior of gas-stress-induced behavior.
5. The strain-based percolation model of permeability evolution under triaxial compression is proposed. The volumetric strain of connected clusters in triaxial compression dominates the transition behavior. The evolution of permeability with volumetric strain shows a good correlation. The results show that the percolation model is very effective at illustrating and predicting the sudden transition behavior of CH<sub>4</sub> seepage in coal by high agreement with the experimental data.

**Author Contributions:** Conceptualization and writing, D.X.; Methodology and software, J.Z. and Y.L.; Visualization, S.Z.

**Funding:** This study was supported by the National Natural Science Foundation of China (grant no. 51504257), the State Key Research Development Program of China (grant no. 2016YFC0600704), the Fund of Yueqi Outstanding Scholars from China University of Mining and Technology (Beijing) (grant no. 2017A03 and 2018A06), and Open Fund of the State Key Laboratory of Coal Mine Disaster Dynamics and Control at Chongqing University (2011DA105287-FW201604).

**Acknowledgments:** We are indebted to Liu at Sichuan University and Jiao at Nanyang Technological University for their critical and constructive review of a preliminary version of this manuscript. We would also like to cordially acknowledge excellent guidance of Zhou and technical work of Wang.

**Conflicts of Interest:** The authors declare no conflict of interest.

## Abbreviations

DS	Dilatant stress (deviatoric stress)
PS	Peak stress (deviatoric stress)
RS	Residual stress (deviatoric stress)
DP	Dilatant permeability
PP	Peak permeability
RP	Residual permeability
DSN	Dilatant strain
PSN	Peak strain
RSN	Residual strain
SDR	Stress drop rate
PCR	Permeability change rate
VCR	Volumetric strain change rate
EDZ	Excavation damaged zone
CT	X-ray computed tomography

## Symbol List

$k, k_0, k_f$	permeability, initial permeability, final permeability
$p_0$	atmospheric pressure, 0.1 MPa
$p_1, p_2$	inlet and outlet gas pressure
$q$	flow rate
$A$	cross-sectional area
$\mu$	gas viscosity coefficient
$L$	length
$F$	fractal set
$A_F^\delta$	parallel body with distance $\delta$

$\delta$	distance
$x_0$	center coordinates
$x, y$	Cartesian coordinates
$vol^n(F_\delta)$	volume in $n$ -dimensional space
$s$	dimension of $F$
$c$	$s$ -dimensional tolerance in set $F$
$v(\delta)$	prism-like volume
$i, j$	grid coordinate
$N_{i,j}$	total amount of volume covering one prism-like volume
$N$	total amount of volume covering all prism-like volume
$D$	damage
$\phi$	porosity
$P$	probability of connectivity
$p$	probability of occupied lattice
$p_c$	critical probability
$\beta$	conductivity index
$\sigma_1, \sigma_3$	maximum and minimum principal stress
$\varepsilon_1, \varepsilon_3$	maximum and minimum principal strain
$\varepsilon_{1D}, \varepsilon_{3D}$	maximum and minimum principal strain at critical dilatant boundary
$C$	a constant obtained from the fitting curve

## References

1. Qin, Y.; Tong, F.; Yang, G.; Mauzerall, D.L. Challenges of using natural gas as a carbon mitigation option in China. *Energy Policy* **2018**, *117*, 457–462. [[CrossRef](#)]
2. Li, H.; Lau, H.C.; Huang, S. China's coalbed methane development: A review of the challenges and opportunities in subsurface and surface engineering. *J. Pet. Sci. Technol.* **2018**, *166*, 621–635. [[CrossRef](#)]
3. Li, Q.; Lin, B.; Zhai, C. A new technique for preventing and controlling coal and gas outburst hazard with pulse hydraulic fracturing: A case study in Yuwu coal mine, China. *Nat. Hazards* **2015**, *75*, 2931–2946. [[CrossRef](#)]
4. Yuan, L. Theory of pressure-relieved gas extraction and technique system of integrated coal production and gas extraction. *J. China Coal Soc.* **2009**, *34*, 1–8.
5. Xue, D.J.; Zhou, H.W.; Chen, C.F.; Jiang, D.Y. A combined method for evaluation and prediction on permeability in coal seams during enhanced methane recovery by pressure-relieved method. *Environ. Earth Sci.* **2015**, *73*, 5963–5974. [[CrossRef](#)]
6. Somerton, W.H.; Söylemezoglu, I.M.; Dudley, R.C. Effect of stress on permeability of coal. *Int. J. Rock. Mech. Min. Sci. Geomech. Abstr.* **1975**, *12*, 129–145. [[CrossRef](#)]
7. Durucan, S.; Edwards, J.S. The effects of stress and fracturing on permeability of coal. *Min. Sci. Technol.* **1986**, *3*, 205–216. [[CrossRef](#)]
8. McKee, C.R.; Bumb, A.C.; Koenig, R.A. Stress-dependent permeability and porosity of coal and other geologic formations. *SPE Form. Eval.* **1988**, *3*, 81–91. [[CrossRef](#)]
9. Seidle, J.P.; Jeansonne, M.W.; Erickson, D.J. Application of matchstick geometry to stress dependent permeability in coals. *Soc. Petrol. Eng. J.* **1992**, 1–11. [[CrossRef](#)]
10. Liu, H.H.; Rutqvist, J.; Berryman, J.G. On the relationship between stress and elastic strain for porous and fractured rock. *Int. J. Rock. Mech. Min. Sci.* **2009**, *46*, 289–296. [[CrossRef](#)]
11. Liu, H.H.; Rutqvist, J. A new coal-permeability model: Internal swelling stress and fracture—Matrix interaction. *Transp. Porous Media* **2010**, *82*, 157–171. [[CrossRef](#)]
12. Shi, J.Q.; Durucan, S. Drawdown induced changes in permeability of coalbeds: A new interpretation of the reservoir response to primary recovery. *Transp. Porous Media* **2004**, *56*, 1–16. [[CrossRef](#)]
13. Witherspoon, P.A.; Wang, J.S.Y.; Iwai, K.; Gale, J.E. Validity of Cubic Law for fluid flow in a deformable rock fracture. *Water Resour. Res.* **1980**, *16*, 1016–1024. [[CrossRef](#)]

14. Valdes-Parada, F.J.; Ochoa-Tapia, J.A.; Alvarez-Ramirez, J. Validity of the permeability Carman–Kozeny equation: A volume averaging approach. *Phys. A Stat. Mech. Appl.* **2009**, *388*, 789–798. [CrossRef]
15. Kruczek, B. Carman–Kozeny Equation. In *Encyclopedia of Membranes*; Springer: Berlin, Germany, 2014; pp. 1–3.
16. Brush, D.J.; Thomson, N.R. Fluid flow in synthetic rough-walled fractures: Navier–Stokes, Stokes, and local cubic law simulations. *Water Resour. Res.* **2003**, *39*, 1–5. [CrossRef]
17. Zhu, W.; Wong, T.F. The transition from brittle faulting to cataclastic flow: Permeability evolution. *J. Geophys. Res. Solid Earth* **1997**, *102*, 3027–3041. [CrossRef]
18. Zhu, W.; Wong, T.F. Network modeling of the evolution of permeability and dilatancy in compact rock. *J. Geophys. Res. Solid Earth* **1999**, *104*, 2963–2971. [CrossRef]
19. Isichenko, M.B. Percolation, statistical topography, and transport in random media. *Rev. Mod. Phys.* **1992**, *64*, 961–1043. [CrossRef]
20. Hunt, A.; Ewing, R.; Ghanbarian, B. *Percolation Theory for Flow in Porous Media*; Springer: Berlin, Germany, 2014.
21. Broadbent, S.R.; Hammersley, J.M. *Percolation Processes: I. Crystals and Mazes*; Cambridge University Press: London, UK, 1957; pp. 629–641.
22. Shante, V.K.S.; Kirkpatrick, S. An introduction to percolation theory. *Adv. Phys.* **1971**, *20*, 325–357. [CrossRef]
23. Chelidze, T.L. Percolation and fracture. *Phys. Earth Planet. Inter.* **1982**, *28*, 93–101. [CrossRef]
24. Bebbington, M.; Vere-Jones, D.; Zheng, X. Percolation Theory: A model for rock fracture? *Geophys. J. Int.* **1990**, *100*, 215–220. [CrossRef]
25. Sahimi, M. Flow phenomena in rocks: From continuum models to fractals, percolation, cellular automata, and simulated annealing. *Rev. Mod. Phys.* **1993**, *65*, 1393–1534. [CrossRef]
26. Alkan, H. Percolation model for dilatancy-induced permeability of the excavation damaged zone in rock salt. *Int. J. Rock Mech. Min. Sci.* **2009**, *46*, 716–724. [CrossRef]
27. ASTM D2664. Standard Test Method for Triaxial Compressive Strength of Undrained Rock Core Specimens without Pore Pressure Measurement. 1986. Available online: <https://www.astm.org/DATABASE.CART/HISTORICAL/D2664-95A.htm> (accessed on 10 August 2018).
28. Hsieh, P.A.; Tracy, J.V.; Neuzil, C.E.; Bredehoeft, J.D.; Silliman, S.E. A transient laboratory method for determining the hydraulic properties of “tight” rocks—I. Theory. *Int. J. Rock Mech. Min. Sci. Geomech. Abstr.* **1981**, *18*, 245–252. [CrossRef]
29. Neuzil, C.E.; Cooley, C.; Silliman, S.E.; Bredehoeft, J.D.; Hsieh, P.A. A transient laboratory method for determining the hydraulic properties of “tight” rocks—II. Application. *Int. J. Rock Mech. Min. Sci. Geomech. Abstr.* **1981**, *18*, 253–258. [CrossRef]
30. Zhou, H.W.; Xue, D.J.; Jiang, D.Y. On fractal dimension of a fracture surface by volume covering method. *Surf. Rev. Lett.* **2014**, *21*, 1–11. [CrossRef]
31. Stauffer, D.; Aharony, A. *Introduction to Percolation Theory: Revised Second Edition*; CRC Press: London, UK, 2014.
32. Sahini, M. *Applications of Percolation Theory*; CRC Press: London, UK, 2014; pp. 23–40.
33. Hestir, K.; Long, J.C.S. Analytical expressions for the permeability of random two-dimensional Poisson fracture networks based on regular lattice percolation and equivalent media theories. *J. Geophys. Res. Solid Earth* **1990**, *95*, 21565–21581. [CrossRef]
34. Sakhaee-Pour, A.; Agrawal, A. Integrating acoustic emission into percolation theory to predict permeability enhancement. *J. Pet. Sci. Eng.* **2018**, *160*, 152–159. [CrossRef]
35. Louis, C. A study of groundwater flow in jointed rock and its influence on the stability of rock masses. *Rock Mech. Res. Rep.* **1969**, *10*, 1–90.
36. Lomize, G.M. Flow in fractured rocks. *Gosenergoizdat* **1951**, *127*, 496. (In Russian)
37. Xue, D.J.; Zhou, H.W.; Liu, Y.T.; Deng, L.S.; Zhang, L. Study of drainage and percolation of nitrogen-water flooding tight coal by NMR Imaging. *Rock Mech. Rock Eng.* **2018**, 1–17. [CrossRef]

